Chapter 1
Fundamentals of Amorphous Systems: Thermodynamic Aspects

Robert A. Bellantone

1.1 Introduction

Drugs with poor aqueous solubility present a major challenge to pharmaceutical scientists because they tend to show low oral bioavailability. This has been one of the most critical issues in pharmaceutical industry for many decades. In 1995, the biopharmaceutical classification system (BCS) was introduced to facilitate drug development, classifying drug molecules according to their solubility and permeability (Amidon et al. 1995). It was estimated that 60–70 % of compounds in development are poorly water soluble. Moreover, it has recently been pointed out that the percentage can be even higher, as high as 90 %, for certain drug categories (Williams et al. 2012).

Pharmaceutical companies screen thousands of new chemical entities (NCEs) every year in the hope to find cures for diseases, but many of these face ill-fated discontinuation partially due to inadequate exposures owing to poor aqueous solubility. In the current environment where only 20–40 NCEs make it to the market (USA) per year (Herschler and Humer 2012), it will be beneficial to the patient and society, even if one or two more compounds are developed annually as medicines by overcoming solubility related issues.

For an orally administered drug to have a therapeutic effect, the drug molecules must be dissolved in the gastrointestinal (GI) fluids, pass through GI membrane to the circulatory system, and reach the target in sufficient quantity. That is, drug molecules must be dissolved in aqueous-based GI fluids in sufficient quantity to have any therapeutic effect. If the solubility of the drug in GI fluids is not sufficient, the bioavailability will be compromised as the absorption will be "solubility limited." It is quite common for poorly soluble compounds to also dissolve slowly. If the dissolution

R. A. Bellantone (✉)
Division of Pharmaceutical Sciences,
Long Island University, Brooklyn, NY, USA
e-mail: Robert.Bellantone@liu.edu

N. Shah et al. (eds.), *Amorphous Solid Dispersions,*
Advances in Delivery Science and Technology, DOI 10.1007/978-1-4939-1598-9_1

rate of the drug is too slow in the timeframe of absorption, the bioavailability will again be compromised as absorption will be "dissolution limited."

It is noteworthy that the mechanism of absorption requires that the drug should be in solution. In this chapter, the term "dissolved" or "in solution" refers to the state in which individual molecules are dispersed in the solvent medium. Complexed or bound molecules such as in micelles, emulsions, drug polymer complexes, or inclusion complexes are excluded from this definition. With this definition, the dissolved form corresponds to the form that is absorbable in vivo. This distinction is important because complexation or other means of solubilization can also increase the apparent dissolved concentration of the drug, but these complexes are not really absorbable "as is" unless they dissociate into individual components.

One way to increase the oral bioavailability is to increase the concentration of the dissolved drug in the GI fluids. This can be achieved by increasing the dissolution rate, increasing the drug solubility, or the combination of both. One of the most remarkable approaches to achieve faster dissolution and higher apparent solubility is converting crystalline drug to amorphous drug (Leuner and Dressman 2002). This amorphous approach has been extensively studied over the past several decades (Simonelli et al. 1969; Chiou and Riegelman 1971; Hancock and Zografi 1997).

Two types of amorphous solids are relevant to the pharmaceutical sciences—pure amorphous material (referred to as neat active pharmaceutical ingredient, or neat API) and solid solutions/dispersions (referred to as amorphous solid dispersions, or ASDs). Both can increase the solubility and dissolution rate, but they are very different microscopically. For a neat API, the material is pure drug and the molecular packing is altered in a manner that weakens the average attractive energy between drug molecules, which in turn lowers the energy barrier for drug molecules to go into solution. On the other hand, in an ASD, the molecular packing is disrupted by dispersing the drug molecules in a solid medium or carrier. Neat amorphous forms will be the subject of this chapter. (ASDs are considered in the next chapter.)

1.1.1 Function of "Dissolved Drugs" in Absorption

The dissolution rate of a drug can be described by the Nernst–Bruner equation

$$\frac{dM}{dt} = k_d(C_S - C) \quad C = \frac{M}{V}, \tag{1.1}$$

where M is the mass of drug dissolved in a volume V of GI fluid, C_s is the solubility of the drug, C is the concentration of the dissolved drug at time t, and k_d is the parameter that depends on factors such as the diffusion coefficient, total surface area, agitation rate, etc. Poorly soluble drugs produce a low level of "dissolved" drug because C_s is inherently low. In addition, dissolution rates tend to be slow for poorly soluble drugs. These factors, as mentioned earlier, make the poorly soluble drug also poorly bioavailable. Taking the concentration C in Eq. (1.1) as the "dissolved" drug concentration in GI fluids, the absorption rate is given by

$$\begin{bmatrix} \text{absorption} \\ \text{rate} \end{bmatrix} = k_a C, \tag{1.2}$$

where k_a is an absorption rate constant that depends on the surface area, membrane permeability, etc. Although Eqs. (1.1) and (1.2) represent an overly simplified version of dissolution of a drug in the GI track, they state that an increasing apparent saturation solubility C_s will improve oral bioavailability by improving the dissolution rate as well.

Despite the aforementioned advantages of amorphous forms, only a few products have been developed using neat API amorphous forms. These include Accolate® (zafirlukast), Accupril® (quinapril hydrochloride), Ceftin® (cefuroxime axetil), and Viracept® (nelfinavir mesylate).

1.2 Structural Aspects

An amorphous solid is characterized by the lack of long-range order symmetry operators (translational, orientational, and conformational order) found in crystalline solid. The absence of long-range order can be ascribed to a random distribution of molecular units. Individual molecules are randomly oriented to one another and exist in a variety of conformational states. The molecular pattern of an amorphous solid is often depicted as that of a frozen liquid with the viscosity of a solid having many internal degrees of freedoms and conformational diversities (disorder). An amorphous solid, at the molecular level, has properties similar to liquids; but at the macroscopic level, it has properties of solids.

The lack of symmetry operators are commonly manifested by the lack of X-ray diffraction peaks typically found in crystalline solid, but may exhibit a characteristic broad amorphous "halo" (Fig. 1.1). In addition, an amorphous solid is further characterized by the lack of distinct melting point and birefringence properties.

The internal molecular arrangement of a solid in general can be projected as a continuum between well-ordered crystalline state and completely disordered amorphous state (Fig. 1.2). A crystalline material is depicted as having three-dimensional long-range symmetry operators over a domain of at least 1000 individual molecules. A mesophase material (liquid crystals, plastic crystals) is depicted as having intermediate symmetry operators, and an amorphous state has no symmetry operators (Klug and Alexander 1974).

Such diverse packing arrangements explain different physicochemical properties of solids, such as differences in density, hardness, thermal properties, conductivity, solubility, etc. In practice, perfect crystals without any defects are not seen, nor are perfect amorphous systems. Recent studies suggest that amorphous solid of small molecules may not be in truly amorphous state but may contain certain structural elements. In fact, amorphous solids can exhibit short-range order over domains that are too small to show crystalline properties (Gavezzotti 2007).

Amorphous solids are considered as glasses, which have rheological properties of solids and molecular properties of liquids (Kittel 1986). The behavior of amorphous glasses can be explained by heat content or molar volume changes with the changes of temperature. When the heat content or molar volume of a sample is plotted against

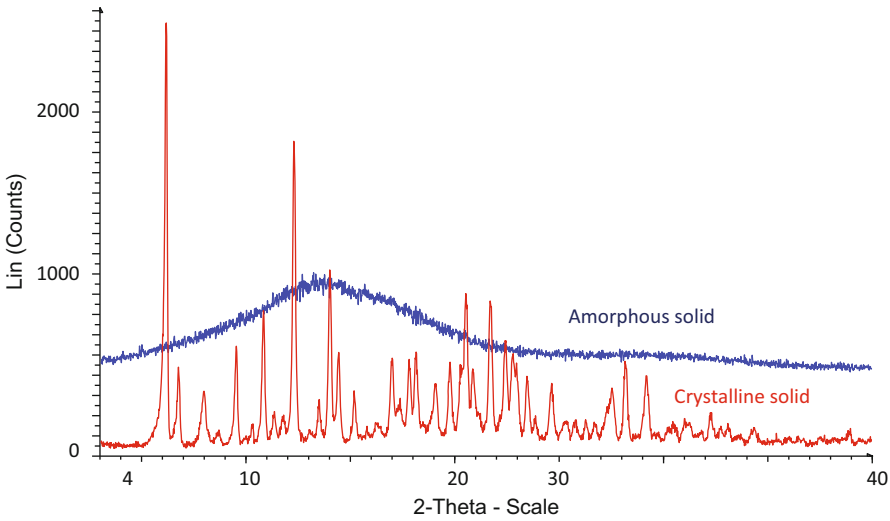

Fig. 1.1 Illustration of X-ray diffraction pattern of crystalline solid (*red*) and amorphous solid (*blue*). Owing to periodic lattice planes, crystalline solid scatters X-ray beam constructively in well-defined directions producing characteristic X-ray diffraction pattern whereas amorphous solid is anisotropic, scatters X-ray beam in many directions producing broad amorphous halos instead of high-intensity narrow peaks

the temperature, these variables change smoothly until it comes to the region known as glass transition temperature, where the variables change abruptly. The temperature region below the glass transition temperature is known as "glassy state" and above the glass transition temperature is known as "rubbery state." The physicochemical and physicomechanical properties of the materials are starkly different between these two regions.

1.3 Thermodynamic Aspects

1.3.1 Two Approaches to Understanding Neat Amorphous Forms

There are two general approaches to understand the behavior of amorphous materials, one based on macroscopic thermodynamic arguments and the other based on microscopic molecular arguments. While these approaches should lead to the same conclusions, each view provides unique ways of explaining material behavior.

Thermodynamics is based on macroscopic observations that characterize average behavior of material based on energy contents. The most fruitful approach is to apply equilibrium thermodynamics, which can be applied even if the system is not in an equilibrium state as long as the intensive variables are uniform within the material. This approach is useful to describe the solubility of the material, in which

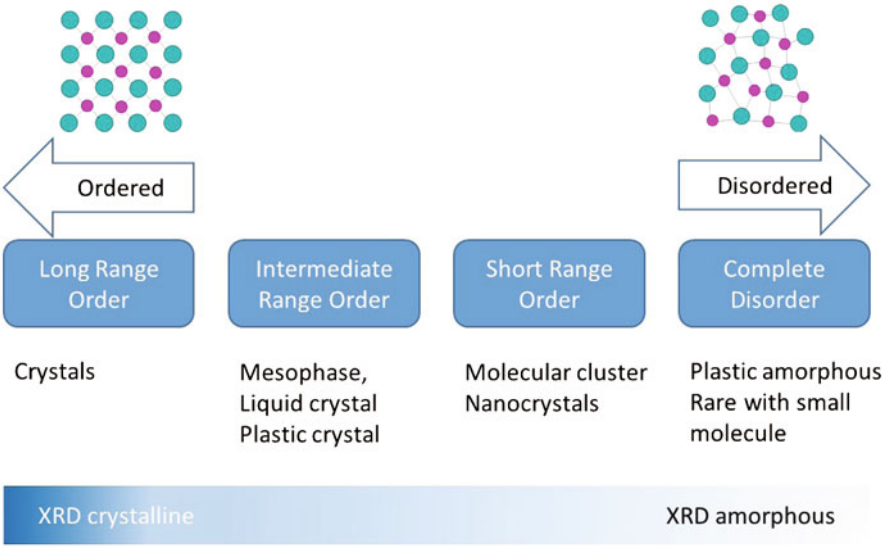

Fig. 1.2 Solid form system illustrating long-range ordered (translational, orientational, and conformational) crystals on one end and completely disordered amorphous material on the other end. Solid forms can assume various length scale of order (long range, medium range, short range) and/or mesomorphic states (smectic, nematic)

the properties of the drug in the dissolved and undissolved forms are be taken into the consideration together.

The material behavior of solid forms is ultimately attributed to the strength of interactions between molecules, which vary significantly depending on the chemical structure and molecular separations. The latter factor is a function of the molecular packing, which sets the distance between molecules. Thus, a microscopic point of view is well suited for a fundamental interpretation of the solid form in terms of molecular interactions and packing.

1.3.2 Description of Forming a Solution

The dissolution process involves removing drug molecules from the undissolved solid and placing them into the holes generated in the solvent system in such a way that molecules are dispersed in the solvent matrix uniformly. In this sense, "undissolved" means the drug is in a solid form and "dissolved" means the drug is molecularly dispersed in a solvent medium. In the undissolved state, the drug molecules interact with each other via various intramolecular cohesive forces to form a condensed solid phase, whereas in the dissolved state, the drug molecules interact with the surrounding solvent molecules.

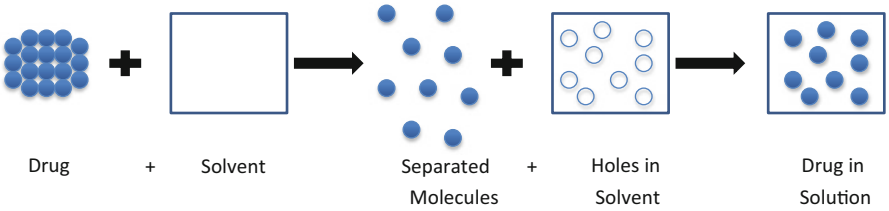

Fig. 1.3 Schematic of dissolution for pure API

Dissolution has been described by a number of models. The ideal solution has been described as a consequence of solute being melted and mixed with the solvent (Atkins 1998). This simplistic view is generalized by adding specific solvent effects in the regular solution theory (Hildebrand and Scott 1950). In particular, the Hildebrand–Scott model includes the differences in interaction energies between the "unmixed" state (drug–drug and solvent–solvent) and the "mixed" or solution state (drug–solvent). A well-known model for calculating these differences is the "hole" model (Martin et al. 1983; Hill 1986). In this model, the drug molecules are separated from the solid and "holes" are generated in the solvent. The drug molecules are then placed in the holes and allowed to migrate until they are uniformly dispersed throughout the solvent as illustrated in Fig. 1.3.

This "hole" model can be depicted as a sequence of conceptual steps as shown below. Because the Gibbs energy is a thermodynamic state function, this sequence of steps does not have to occur in reality, but it provides a means to calculate the changes in Gibbs free energy due to dissolution (Klotz and Rosenberg 1974). As the changes in Gibbs energy only depend on the final state and the initial states, this is analogous to "Hess' law" of thermodynamics (Atkins 1998).

Assuming the temperature and pressure (*T, P*) remain constant, dissolving a solid drug in a liquid solvent can be modeled by the following sequence.

1. Break up the lattice structure of the solid to supercooled liquid at (*T, P*).
2. Separate the molecules from the supercooled liquid at (*T, P*).
3. Make uniformly distributed "holes," one for each drug molecule, in the solvent at (*T, P*).
4. Put the drug molecules in the holes at (*T, P*).

Steps 1–3 require an input of energy to overcome the drug–drug molecular attractions to separate them, and to overcome solvent–solvent molecular attractions to create holes within the solvent. In step 4, energy is given back as a result of drug–solvent molecular attractions.

Figure 1.4 illustrates a diagram of the Gibbs energy versus the dissolution process at a given (*T, P*). The diagram includes the initial raw material state of undissolved drug and solvent (A), the final solution state of the drug dissolved in the solvent (D), and two hypothetical intermediate states B and C. The changes of Gibbs energy by forming the solution, ΔG_S, are the Gibbs energy of state D minus state A. For state

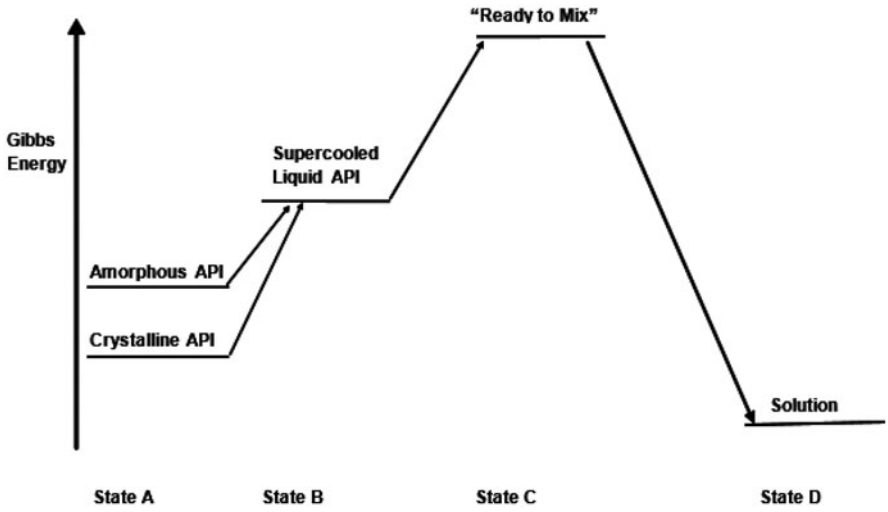

Fig. 1.4 Gibbs energy diagram for the dissolution scheme. *State A* represents the initial state consisting of undissolved solid API and empty solvent. *State B* represents a supercooled liquid API plus empty solvent. *State C* represents separated drug molecules and holes in the solvent. *State D* represents the final solution in which the drug is dissolved in the solvent

A, two initial states are shown—one in which the undissolved API is crystalline, and another in the amorphous form.

The intermediate state B represents the "empty" solvent and "supercooled" liquid API. For a given amount of API at (*T, P*), all liquid forms of API (including supercooled) have the same Gibbs energy regardless of the starting solid form in state A. State C is another intermediate state in which the drug molecules have been separated and uniformly distributed holes have been made in the solvent, in which the number of holes equals to the number of separated drug molecules. This can be thought of as a "ready to mix" (RTM) state, and the energy level is also the same regardless of the starting undissolved drug forms. The RTM state also represents the highest Gibbs energy level in the overall dissolution processes.

With the assumption that all drug molecules in state A dissolve, the Gibbs energy level in the final solution is independent of the starting solid forms. Thus, the energy differences between states B, C, and D are independent of the starting undissolved solid form of state A . However, the energy required to pass from state A to state B does depend on the starting solid form, and is less for the amorphous than the crystalline form. In this regard, state B serves as a reference point, especially with regard to the energy of state A, which reflects different energies for different starting forms.

As depicted in Fig. 1.4, the difference between the initial and final Gibbs energy levels (state D minus state A) ΔG_S dictates the solubility of the drug in the solvent. The difference between the initial energy levels and the intermediate RTM state energy level (state C minus state A) represents the energy required to bring the system

to the dissolved state. This can be thought of as analogous to an energy barrier or activation energy for dissolution, which is related to the kinetics of dissolution. It should be noted that this is not the only factor affecting dissolution rates. Thus, because of smaller activation energy, material with higher initial energy levels will result in higher solubility and faster dissolution. Since amorphous systems start at a higher level than crystalline forms (level A), the reduced energy barrier (activation energy) partially explains why the kinetics of dissolution is faster for amorphous systems.

1.3.3 Calculating the Gibbs Energy Change ΔG_S of Forming a Solution

The change in Gibbs energy due to dissolving the solid, ΔG_S, is the sum of changes for each step. If the starting and ending (T, P) are the same, it can be shown that (Bellantone et al. 2012)

$$\Delta G_S = \sum \Delta H - T \sum \Delta S, \tag{1.3}$$

Thus, ΔG_S can be calculated by finding the changes in enthalpy and entropy from steps 1–4 above and inserting them into Eq. (1.3), as illustrated below.

Step 1 can be modeled as follows. At constant pressure, the ΔH is given by (1) the heat required to bring the solid from T to its melting temperature T_{M1}, (2) melting the solid at that temperature, and then (3) cool the melt as a supercooled liquid back to the original temperature:

$$\Delta H(1) = \int_T^{T_{M1}} n_1 C_{P1}^{(S)} dT + n_1 \Delta h_{M1} + \int_{T_{M1}}^{T} n_1 C_{P1}^{(L)} dT, \tag{1.4}$$

where n_1 represents the moles of drug, $C_{P1}^{(S)}$ and $C_{P1}^{(L)}$ represent the molar heat capacities of the solid and supercooled liquid melt, respectively, and Δh_{M1} represents the molar heat of melting of the drug. In general, $C_{P1}^{(S)}$, $C_{P1}^{(L)}$, and ΔC_{P1} are functions of the temperature, so they are brought into the integral. Noting that $dS = (C_P/T)dT$ and $\Delta S_{M1} = \Delta H_{M1}/T_{M1}$, and defining $\Delta C_{P1} = C_{P1}^{(S)} - C_{P1}^{(L)}$, the enthalpy and entropy changes associated with step 1 are:

$$\Delta H(1) = n_1 \Delta h_{M1} + n_1 \int_T^{T_{M1}} \Delta C_{P1} dT \quad \Delta S(1) = \frac{n_1 \Delta h_{M1}}{T_{M1}} + \int_T^{T_{M1}} \frac{n_1 \Delta C_{P1}}{T} dT, \tag{1.5}$$

The enthalpic contributions from steps 2–4 are typically combined to give a total enthalpy of mixing ΔH_{mix}, which represents the net total of the energy input to separate the drug molecules and to make holes in the solvent, minus the energy

released due to drug–solvent interactions. For regular solutions, this is often modeled as

$$\Delta H_{mix} = n_1 x_0 \chi RT, \tag{1.6}$$

where $x_0 = n_0/(n_1+n_0)$ is the mole fraction of the solvent. The interaction parameter χ has been modeled theoretically in terms of solubility parameters as

$$\chi = \frac{V_{m,1}\phi_0^2}{RT}(\delta_1 - \delta_0)^2, \tag{1.7}$$

where δ_1 and δ_0 represent the solubility parameters of the drug and solvent, respectively, $V_{m,1}$ is the molar volume of the drug, and ϕ_0 represents the volume fraction of the solvent (which is very close to 1 for dilute solutions). Equation (1.7) has limitations because it requires the heat of solution to be always positive, which conflicts with observations that they can be positive (endothermic) or negative (exothermic). Extensions have been proposed to correct for this, such as (Adjei et al. 1980)

$$\chi = \frac{V_{m,1}\phi_0^2}{RT}\left(\delta_1^2 + \delta_0^2 - 2W\right), \tag{1.8}$$

in which the parameter W can allow for negative values of the interaction parameter.

In step 3, choosing the holes to be uniformly distributed in the solvent ensures that the molecules spread out to achieve a uniform average concentration. This is part of the entropy of mixing ΔS_{mix}, which accounts for the spreading out of the drug molecules when they go from the condensed phase (liquid or solid) into solution, and is given by (Atkins 1998)

$$\Delta S_{mix} = -R[n_1 \ln x_1 + n_0 \ln x_0], \tag{1.9}$$

where $x_1 = n_1/(n_1 + n_0)$ denotes the mole fraction of the drug in solution. As $x_1 + x_0 = 1$, each log term is less than one and $\Delta S_{mix} > 0$. It is assumed that this is the only entropy effect due to mixing. (Although not considered for the purposes of this discussion, there can be other sources of entropy change on mixing. For instance, water molecules orient around drugs that are polar or ionic, which would result in a loss of entropy that would be taken into account along with an adjusted the entropy of mixing.)

The change in Gibbs energy that results from dissolving a drug in a solvent is

$$\Delta G_S = G(\text{solution}) - G(\text{unmixed components}), \tag{1.10}$$

Adding the contributions from steps 1–4 gives

$$\Delta G_S = n_1 \Delta h_{M1}\left(1 - \frac{T}{T_{M1}}\right) + n_1 \int_T^{T_{M1}} \Delta C_{P1} dT \tag{1.11}$$

$$- n_1 T \int_T^{T_{M1}} \frac{\Delta C_{P1}}{T} dT + n_1 x_0 \chi RT + RT[n_1 \ln x_1 + n_0 \ln x_0].$$

For drugs dissolving in liquid solvents, the heat capacity terms in Eq. (1.11) are relatively small compared to the heat of melting terms and can be neglected. In some models, they are not neglected but the $\Delta C_{P,1}$ term is taken as constant. While both of these approximations can introduce errors, the heat capacity terms will be neglected in the discussion that follows in order to simplify the equations and highlight the principles, so Eq. (1.11) will be replaced by the simpler form:

$$\Delta G_S = n_1 \Delta h_{M1} \left(1 - \frac{T}{T_{M1}}\right) + n_1 x_0 \chi RT + RT[n_1 \ \ln \ x_1 + n_0 \ \ln \ x_0]. \quad (1.12)$$

It should be noted that the effects of the heat capacities can be especially important when modeling solid solution ASDs (Bellantone et al. 2012).

1.3.4 Solubility and Chemical Potential

From thermodynamics, it is well established that materials will convert from a higher to lower chemical potential form. In this context, the chemical potentials of the drug in its dissolved and undissolved states are of primary interest. The chemical potential of a drug is the change in the Gibbs energy per changes in drug amount, holding all other factors (remaining chemical composition, temperature, and pressure) constant. This is written as (Atkins 1998)

$$\mu_1 = \left(\frac{\partial G}{\partial n_1}\right)_{T,P,n_0}. \quad (1.13)$$

The change in chemical potential for the drug due to dissolution is given by

$$\Delta\mu_1 = \begin{bmatrix} \text{chemical potential of} \\ \text{dissolved drug} \end{bmatrix} - \begin{bmatrix} \text{chemical potential} \\ \text{of undissolved drug} \end{bmatrix}. \quad (1.14)$$

From Eq. (1.13), this is given by (Bellantone et al. 2012)

$$\Delta\mu_1 = \left(\frac{\partial \Delta G_S}{\partial n_1}\right)_{T,P,n_0}. \quad (1.15)$$

When chemical potential of the undissolved drug is higher than that of the dissolved drug, $\Delta\mu_1 < 0$, the solution is below saturation, and more drug can dissolve if present. On the other hand, if the chemical potential of the dissolved form is higher than the undissolved form, $\Delta\mu_1 > 0$ and the solution is supersaturated, and precipitation is favored. The solubility of the drug in a solvent can be taken as the dissolved concentration at which $\Delta\mu_1 = 0$.

Equation (1.15) is important because it shows that $\Delta\mu_1$ represents the slope of ΔG_S versus the moles of drug "dissolved" (both per constant amount of solvent), which is shown in Fig. 1.5. The solubility criterion of $\Delta\mu_1 = 0$ corresponds to

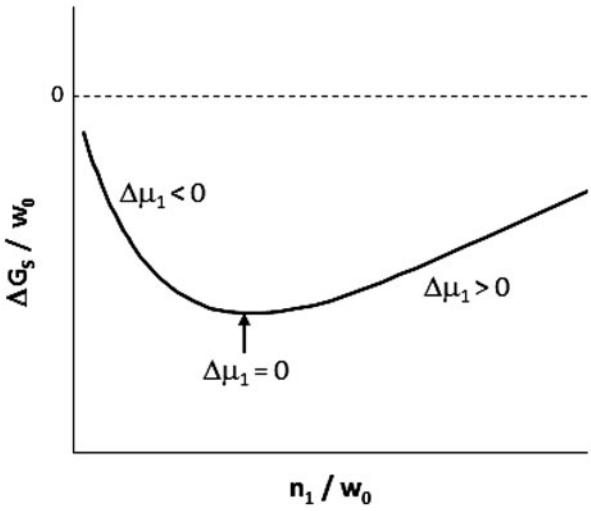

Fig. 1.5 Change in Gibbs energy versus moles of dissolved drug (both per gram of solvent)

the minimum of the plot, where the slope is zero, and the solubility is taken as n_1/w_0 (which can then be converted to other units). To the left, corresponding to lower amounts of dissolved drug, the dissolved concentration is below the solubility ($\Delta\mu_1 < 0$), and to the right it is supersaturated ($\Delta\mu_1 > 0$).

Noting that the mole fractions of the dissolved drug and solvent are given by $x_1 = n_1/(n_1 + n_0)$ and $x_0 = n_0/(n_1 + n_0)$, respectively, applying the derivative in Eq. (1.15) to Eq. (1.12) leads to

$$\Delta\mu_1 = \Delta h_{M1}\left(1 - \frac{T}{T_{M1}}\right) + x_0^2 \chi RT + RT \ \ln \ x_1. \tag{1.16}$$

Since $0 < x_1 < 1$, the left-hand side of Eq. (1.16) is negative when the "dissolved" concentration x_1 is low, but becomes less negative as the dissolved drug concentration increases. Figure 1.6 shows a plot of Eq. (1.16), in which $\Delta\mu_1$ is negative for dissolved concentrations below the solubility, equals zero when the "dissolved" concentration equals the solubility, and is positive for supersaturated solutions. Equation (1.16) can be simplified for dilute solutions by noting that x_0^2 is very close to 1. Doing this and setting $\Delta\mu_1 = 0$, the drug solubility x_{1S} is obtained as

$$\ln \ x_{1S} = -\frac{\Delta h_{M1}}{RT} - \chi + \frac{\Delta h_{M1}}{RT_{M1}}. \tag{1.17}$$

Equation (1.17) can be equivalently written in terms of an activity coefficient γ_1 instead of the interaction parameter χ as

$$\ln \ x_{1S} + \chi = \ln \ \gamma_1 x_{1S} = \frac{\Delta h_{M1}}{R}\left(\frac{1}{T_{M1}} - \frac{1}{T}\right), \quad \text{where } \ln \ \gamma_1 = \chi. \tag{1.18}$$

Figure 1.6 shows the effect of the chemical potential change on solubility. It can be seen that the solubility increases exponentially with the increase in chemical

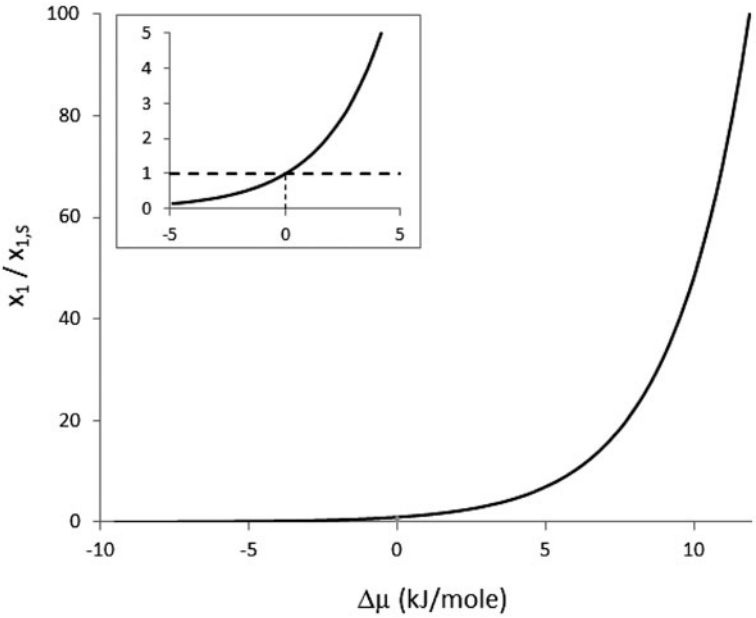

Fig. 1.6 Concentration versus chemical potential change

potential, and for $\Delta\mu_1 > 0$, even small increases in the chemical potential result in very large increases in the solubility.

The dotted line in the insert represents the solubility of the stable crystalline drug form.

1.3.5 Amorphous Versus Crystalline Form Solubility

For a given drug and solvent at (*T, P*), the chemical potential of the dissolved drug is determined by the concentrations of the components. On the other hand, the chemical potential of the undissolved drug is a function of a number of parameters that can be altered, including the molecular arrangement.

The solubility of the drug in terms of mole fraction is given by Eq. (1.17). Any factor that makes the right-hand side of Eq. (1.17) more positive (or less negative) will work to increase the solubility of the drug. For a given drug and solvent, physical factors that influence the right-hand side include the heat of melting Δh_{M1} and the melting temperature T_{M1} of the "undissolved" solid form, both of which are different for the amorphous versus crystalline forms. The effect can be seen as follows. The solubility (mole fraction), heat of melting, and melting temperature for the amorphous form will be denoted as x_S^A, Δh_{M1}^A, and T_{M1}^A, respectively, and the analogous parameters for the most stable crystalline form will be denoted using the superscript

"C." The solubility with respect to each form is given by Eq. (1.17), using the appropriate mole fraction, heat of melting, and melting temperature. Thus, subtracting $\ln x_{1S}^{(A)} - \ln x_{1S}^{(C)}$ gives

$$\ln \frac{x_{1S}^{A}}{x_{1S}^{C}} = -\frac{\left(\Delta h_{M1}^{A} - \Delta h_{M1}^{C}\right)}{RT} + \left(\frac{\Delta h_{M1}^{A}}{RT_{M1}^{A}} - \frac{\Delta h_{M1}^{C}}{RT_{M1}^{C}}\right) = -\frac{\delta h_{M1}}{RT} + \frac{\delta s_{M1}}{R}, \quad (1.19)$$

where $\delta h_{M1} = \left(\Delta h_{M1}^{A} - \Delta h_{M1}^{C}\right)$ and $\delta s_{M1} = \left(\Delta h_{M1}^{A}/T_{M1}^{A} - \Delta h_{M1}^{C}/T_{M1}^{C}\right)$. It is noteworthy that χ does not appear in Eq. (1.19), which reflects the fact that the "dissolved" drug molecules interact with the solvent in the same way regardless of the "undissolved" solid form. From Eq. (1.19), any effect that makes the right-hand side more positive will result in an increase in the relative solubility $x_{1S}^{(A)}$ vs. $x_{1S}^{(C)}$. Since the left-hand side of Eq. (1.19) is positive, a constraint is imposed on the right-hand side in that $\delta s_{M1} > 0$ is required for all amorphous systems, which says that the amorphous form will have higher entropy than the crystalline form.

Solubility information can be applied to the solid-state forms as well, since the relative solubilities of two forms will also give the difference in chemical potential between them in the solid state. Denoting the difference in the chemical potentials between forms as $\delta\mu = \mu_{1S}^{A} - \mu_{1S}^{C}$, Eq. (1.19) leads to

$$\delta\mu = RT \ln \frac{x_{1S}^{A}}{x_{1S}^{C}}. \quad (1.20)$$

Thus, a solid form that displays a higher solubility than the crystalline form must also display a higher chemical potential. Since material tends to move or convert from higher chemical potential to lower chemical potential forms, the form with the lower chemical potential is more stable, verifying that the more stable form will also have a lower solubility.

It is possible to show that the amorphous form is less stable than any crystalline form over all temperatures by considering the following. From Eqs. (1.19) and (1.20), the relative stability of the amorphous or any polymorph compared to the more stable form, as given by $\delta\mu$, depends on the temperature. Polymorph pairs can be classified as either monotropic or enantiotropic. A monotropic pair is one in which one form is more stable at all temperatures up to the melting temperature of the less stable form. An enantiotropic pair is one in which there is a crossover or transition temperature T_X such that for temperatures lower than T_X one form is more stable while above T_X the other form is more stable. An implied requirement for enantiotropic pairs is that neither form melts below the crossover temperature, otherwise, the pair would be monotropic. (Once melted, there is no solid structure, so there can be no amorphous or polymorphic properties.)

Several rules of thumb have been identified (Burger and Ramberger 1979) to help predict whether a pair is monotropic or enantiotropic. One can be illustrated in terms of the melting temperatures and melting enthalpies as follows. Consider two forms, A and C, where form C has the higher melting temperature. The transition temperature

T_X is defined as the temperature at which the chemical potential of the two forms is equal, so $\ln\left(x_{1S}^A/x_{1S}^C\right) = 0$ and Eq. (1.19) leads to

$$T_X = \frac{\left(\Delta h_{M1}^A - \Delta h_{M1}^C\right)}{\left(\frac{\Delta h_m^A}{T_{M1}^A} - \frac{\Delta h_m^C}{T_{M1}^C}\right)} = \frac{\left(\Delta h_{M1}^A - \Delta h_{M1}^C\right) T_{M1}^A T_{M1}^C}{\left(\Delta h_{M1}^A T_{M1}^C - \Delta h_{M1}^C T_{M1}^A\right)}. \tag{1.21}$$

Noting that T_{M1}^C denotes the higher melting point and defining $\delta T_{M1} = T_{M1}^A - T_{M1}^C < 0$, Eq. (1.21) can be rewritten as

$$\frac{T_X}{T_{M1}^A} = \frac{\delta h_{M1} T_{M1}^C}{\delta h_{M1} T_{M1}^C - \Delta h_{M1}^C \delta T_{M1}} = \left(1 - \frac{\Delta h_{M1}^C}{\delta h_{M1}} \frac{\delta T_{M1}}{T_{M1}^C}\right)^{-1}. \tag{1.22}$$

Since δT_{M1} is negative by convention while the heat of melting and melting temperature Δh_{M1}^C and T_{M1}^C are positive, $T_X/T_{M1}^A < 1$ when δh_{M1} is positive, and $T_X/T_{M1}^A > 1$ when δh_{M1} is negative. In other words, if $\Delta h_{M1}^C < \Delta h_{M1}^A$ (so $\delta h_{M1} > 0$) it is predicted that the transition temperature is below the melting point of the less stable form, or $T_X < T_{M1}^A$, which is characteristic of an enantiotropic pair. On the other hand, if $\Delta h_{M1}^C > \Delta h_{M1}^A$ (so $\delta h_{M1} < 0$) it is predicted that $T_X > T_{M1}^B$, so form C is more stable at all temperatures below the melting point of form A and the pair is monotropic. This leads to what Burger and Ramberger (1979) term the heat of fusion (HFR) rule: When the form with the higher melting temperature has the lower heat of melting, the forms are usually enantiotropic, otherwise they are monotropic. Thus, since amorphous solids display lower melting temperatures and heats of melting than the crystalline forms, amorphous solids are less stable at all temperatures than the crystalline forms.

1.4 The Microscopic View

In addition to thermodynamic and macroscopic models, the behavior of amorphous systems can be viewed in terms of microscopic and molecular arguments. While these are equivalent in theory, each view provides different insights and advantages for explaining certain behaviors. In particular, the microscopic viewpoint allows a fundamental interpretation in terms of molecular interactions and packing, while thermodynamics allows material-independent equations to be developed based on macroscopic energy content arguments.

From the standpoint of dissolution, the microscopic viewpoint allows a simple but useful picture to be constructed that gives a clear and intuitive way to think of the properties of amorphous systems with regard to dissolution. When a solid drug dissolves, molecules leave the solid matrix and disperse in the solvent, which can be thought of as resulting from several processes. (1) Solvent molecules interact and associate with drug molecules on the solid surface. (2) Energy is released in the form of heat due to the solvation. (3) The heat energy that is released helps the molecule leave the solid pack and migrate into the solvent, where solvent molecules surround it.

From this point of view, a number of factors can influence the dissolution rate. (1) Stronger attractive forces between the solvent and drug molecules result in releasing more heat of solvation, which will increase the rate at which undissolved molecules can pass into the solvent. (2) For a given drug and solvent, physical forms of undissolved solids with reduced drug–drug attractions will make it easier to remove drug molecules from the undissolved form. This is the dominant effect in explaining the increased dissolution and solubility of amorphous forms compared with crystalline forms. Presumably, molecules in the amorphous form show weaker attractive forces and more easily give up molecules from the solid surface to the solvent medium. (3) The addition of heat will increase the dissolution or solubility by making it easier for the solvent to remove drug molecules from the undissolved environment. These effects have been described thermodynamically in the previous section, but can also be described in molecular terms based on separations and intermolecular attractions and the total kinetic energy of the molecules.

Another property of amorphous forms is that they are not physically stable, and tend to transform into crystalline forms over time. This is almost always accompanied by an increase in density, indicating that the molecules in the crystalline form are arranged more densely on average than in the amorphous form.

All of these can be explained using molecular interaction models, and these are in fact the basis of computational research done today. The basic ideas and how they explain observed behaviors are discussed below.

1.4.1 Interaction Versus Total Energy

The properties of amorphous materials can be explained to a great extent by considering intermolecular interactions such as van der Waals and dipolar interactions, and kinetic energy associated with molecular motion. In the discussions that follow, the standard convention for energies and forces are used. Negative energies denote situations in which energy must be added to separate molecules. Negative forces denote attraction, so molecules move closer to reduce their separation, while positive forces values are repulsive.

Molecular interactions have been described for both neutral and ionic cases. The former case includes hydrogen bonding and weaker van der Waals interactions (dipole/dipole, dipole/induced-dipole, and induced-dipole/induced dipole). In all of these cases, the interactions are attractive unless the molecules are forced so close that electron cloud overlap creates a repulsion. For poorly soluble drugs, the neutral interactions are typically considered most important, but it has recently been shown that coulombic (ionic) interactions also contribute to the total intermolecular interactions (Gavezzotti 2007). However, to illustrate the molecular concepts, this discussion will focus on neutral interactions.

Neutral interactions can be qualitatively described as a function of distance between molecules. While this concept is straightforward for atoms and simple

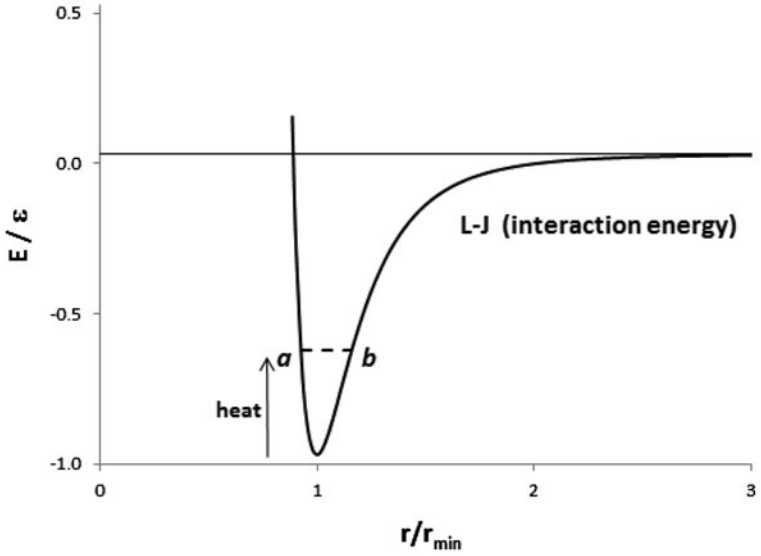

Fig. 1.7 Typical dependence of pairwise energy versus separation

molecules, it is less so for organic molecules owing to the complexity of the molecule, which requires that orientation be taken into account. In this case, the distance between molecules can be considered an average quantity naturally related to the number of molecules per unit volume, which is the density of a substance. The distance between molecules can be thought of as roughly a center-to-center distance for simple molecules, but it is understood that this is a crude approximation for more complicated organic molecules.

It is well established that molecules repel each other when they are brought close together and attract when separated by larger distances. A number of models have been proposed to describe these interactions. For the purposes of this discussion, the exact equation is not of primary concern, but rather the general features of the interaction plot. However, it is often the case for pairs of simple molecules separated by a distance r that the repulsive interaction energy can be described as a/r^m, and the attractive energies can be described by $-b/r^n$. The total interaction energy E_{int} is the sum of the two, resulting in positive interaction energy at small separations, a separation at which the interaction energy is most negative, and zero interaction when molecules are separated by large distance. This behavior is shown in Fig. 1.7 for the Lennard-Jones (L-J) model (Atkins 1998; Hill 1986), which is one of the most studied interaction models. The L-J model gives the interaction energy as

$$E_{\text{int}} = \varepsilon \left[\left(\frac{r_{\min}}{r} \right)^{12} - 2 \left(\frac{r_{\min}}{r} \right)^{6} \right]. \tag{1.23}$$

The greatest attractive energy occurs at the minimum of the plot, where $E_{\text{int}} = -\varepsilon$ and the separation is $r = r_{\min}$. The separation at which $E_{\text{int}} = 0$, which occurs at the intersection of the L-J plot and the horizontal zero line, is denoted by r_0, so the interaction energy for the molecule pair is negative for $r > r_0$. The interaction force is $F_{\text{int}} = -\partial E_{\text{int}}/\partial r$, which is the negative of the slope of the E_{int} versus r plot. Since a negative slope corresponds to a repulsive force, the force between the molecules is repulsive when the separation is less than $r_{\min}$ and attractive when it is greater. At $r = r_{\min}$, the slope is zero and there is no net force due to interactions between the pair of molecules.

The L-J curve shown in Fig. 1.7 denotes only the potential energy between two molecules because the interaction energy does not include kinetic energy, so it represents the total energy of the pair only when there is no heat content, which occurs at absolute zero ($T = 0$ K). In that case, the molecules can be thought of as being at constant positions and the separation distances between molecules do not change.

When heat is added, the total energy of the pair will increase by a quantity equal to the heat added, so the molecules acquire kinetic energy and move relative to each other. Figure 1.7 shows an example in which heat is added to a molecular pair initially separated by $r_{\min}$. The arrow shows the increase in energy to the level denoted by line segment *a–b,* and the corresponding energy will be denoted by E_{ab}. Since $E_{ab} < 0$, the separation between molecules will remain finite and the pair will oscillate at that energy along the line segment between points *a* and *b,* which correspond to the minimum and maximum separations r_a and r_b. As the molecules approach each other, they will slow as they approach and stop when they reach separation r_a, then begin to move apart because of a repulsive force at that distance. Similarly, as they are moving apart, they will slow as they approach and stop at r_b, then begin to move closer because of the attractive force at that separation.

As depicted in Fig. 1.7, the potential energy graph for real systems is not typically symmetric about $r_{\min}$, so at energy E_{ab} the magnitude of displacement from the minimum is smaller for $r_{\min} - r_a$ than $r_b - r_{\min}$. An important consequence of this asymmetry is that the average separation increases when heat is added, which results in thermal expansion. (It should be noted that this is the average position over time, which is greater than the simple average of r_a and r_b.)

1.4.2 Extension to Macroscopic Systems

Organic molecules do not follow the L-J model exactly, but typically behave in a qualitatively similar manner. For instance, the L-J model describes interactions between pairs of molecules, so each molecule experiences the effects from other molecule as a function of the distance r. In bulk solids, individual molecules are surrounded by multiple neighboring molecules at specific locations with thermal motion (for $T > 0$). Thus, a distance of a molecule "*j*" to adjacent molecules "*k*" may vary depending on location, which are time dependent and denoted as $r_{jk}(t)$. However, because the interactions decrease as $1/r^6$, their magnitude drops sharply

with even small increases in distance, so the sum is typically required only over the nearest neighbor molecules (i.e., the first "layer" or so of neighbors surrounding the molecule).

Despite qualitative similarities, organic molecules deviate from the L-J model as a consequence of molecular arrangements. A large number of adjacent molecules mean that the total interaction energy will be complex and of larger magnitude. In addition, the L-J model is one-dimensional (1-d), while molecular packing of real materials occur in three dimensions (even though on surfaces may not be surrounded from all directions). Since energies and forces are additive, the total interaction energy and force felt by molecule "*j*" are additive and summed over all nearest neighbors "*k,*" as

$$E_{\text{int}}^{Tot}(j) = \sum_{k} E_{\text{int}}(r_{jk}) \quad \text{and} \quad F_{\text{int}}^{Tot}(i) = \sum_{j} F_{\text{int}}(r_{ij}). \tag{1.24}$$

At temperature above absolute zero, molecules have kinetic energy. Thus, their positions and corresponding distance $r_{jk}(t)$ vary with time, so the sums in Eq. (1.24) are extremely complicated and must be done using computational models such as molecular dynamics simulations (Gavezzotti 2007). In addition, when the molecules are moving relative to one another, the average vibrational amplitude becomes important. For instance, at low temperatures, the amplitudes are small, and the molecules are vibrating about average locations that are approximately fixed. However, when the average amplitude becomes similar to the average molecular separation, molecules can begin changing places so their "average" position changes with time. When this occurs for a sufficient fraction of the molecules, the solid transforms into a melt. It is significant that this is a consequence of three-dimensional packing and motion. (In the L-J model, which is one-dimensional in *r*, switching locations would require molecules going through zero separation, which would require infinite energy in theory. Thus, there is no corresponding concept in 1-d.)

With these considerations in mind, a hypothetical behavior of a neat API sample is shown in Fig. 1.8, which plots the potential energy versus the average distance as a dotted-solid line combination (through *e-a-b-d-f*). This line will not be exactly proportional to any L-J curve because the relative positions of the molecules in 3-d will change as a result of thermal expansion. The curved line containing points *b* and *c* represents the time-average molecular distance $\langle r \rangle$, which increases with increasing heat content as a reflection of thermal expansion. Along the vertical axis, level *A* corresponds to the energy content at absolute zero and level *B* corresponds to the energy after adding some quantity of heat.

The line segment *a–d* represents the average minimum-to-maximum separations between molecules, which approximately corresponds to the average vibrational amplitude in 3-d for molecules in a sample with that heat content. Of particular interest is the length of *a–d* compared to the average separation $\langle r \rangle = c$. In this example, the energy level *B* was chosen so the length of *a–d* is similar to the value of *c,* so the average vibrational amplitude is comparable to the average separation. Thus, level *B* corresponds to where the solid transitions to the melt phase, and the difference between levels *B* and *A* is the heat of melting.

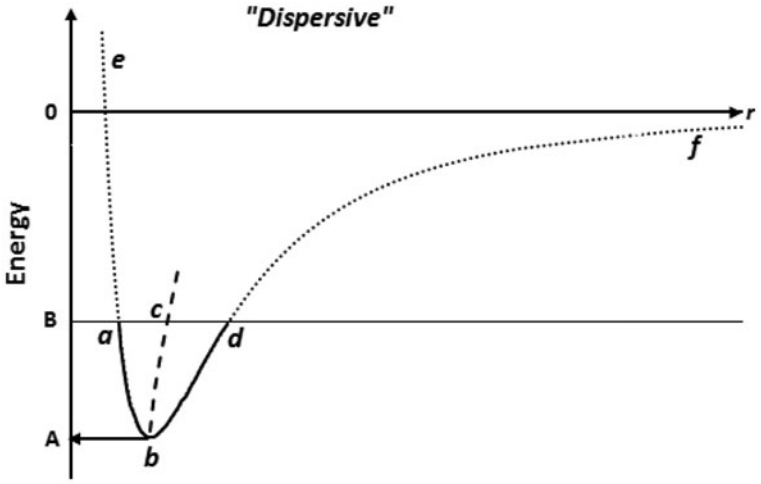

Fig. 1.8 Typical dependence of energy versus the average separation. The *dotted-solid line* (*e-a-b-d-f*) represents the average total attractive interaction energy experienced by a molecule potential versus the average separation between molecules. The *dashed line* going through the points *b* and *c* represents the average molecular separation at each energy level. The *line segment a–d* represents the average vibrational amplitude of molecules with total energy *B*, and point *c* represents the average separation. The energy difference between levels *B* and *A* represents the heat added to melt the material

Several comments are warranted. First, the heat of melting in this example was taken relative to a reference state of absolute zero. The heat of melting for samples at higher temperatures with energy levels higher than *A* is represented by the difference between level *B* and the new starting level. Second, although the example shown here assigned the melting energy at the level for which the length of *a–d* equals the average separation *c,* this is a crude approximation for illustration only. Although the molecular mobility increases dramatically when the vibrational amplitude becomes similar to the average separation, the exact ratio is difficult to determine and will require the use of molecular dynamics or similar approaches.

Third, unless the melt is supercooled, for a given temperature and heat content, the energy level *B* becomes a reference point. This is because the melt has no long-range structure and should contain the same energy content regardless of the starting solid form. Thus, different solid forms will show different energy shapes along points *e–a–b–d–f* and different lengths *a–d*, with more stable forms showing level *A* more negative than for less stable forms, but with the same level *B* energy. In fact, the amorphous form, which would be least stable, would have the highest (least negative) energy value at absolute zero.

The difference in energy between level *B* and the zero line corresponds to the energy that must be added to reach the dispersive region, in which the total energy for the molecules is greater than zero. This corresponds to the case in which the kinetic energy is sufficient to overcome the negative interaction energy due to molecular

attractions, so the molecules are free to "spread out." Since the energy content of the melted form at a given temperature and pressure does not depend on the starting form, the heat energy required to go from level *B* into the dispersive region is constant for a given (*T, P*).

Finally, as more heat is added to solids with energy below level *B,* more modes of vibration become available and the average amplitude of the vibrations increases, so the kinetic energy increases from two sources. Thus, the change in kinetic energy with change in temperature is not constant. This is reflected by the fact that heat capacities tend to increase with increased temperature.

1.5 Glasses and Amorphous Forms

An amorphous solid form is often considered to be equivalent to glass form. A glass can be thought of as a supercooled liquid lacking long-range molecular packing order but with rheological properties of a solid. The viscosity η of liquid increases as the temperature is decreased. Depending on the cooling rate and compound properties, some melts crystallize when cooled below melting temperature, while others may remain as supercooled liquids. For those that crystallize, the viscosity increases drastically due to the phase transition. For those that survive as supercooled liquids, the viscosity increase is in continuum with the decreasing temperature over some temperature range till it reaches the glass transition temperature, at which the viscosity increases typically by 6 orders of magnitude or more over temperature range of typically 5–10°C. This is shown in Fig. 1.9 for supercooled liquids, which shows log η versus the temperature.

The viscosity is strongly related to timeframes for molecular motions or relaxations, which are characterized by an average relaxation time τ that is temperature dependent (Donth 2001; Yu 2001). In particular, systems that respond quickly to deviations from equilibrium, such as an applied stress, are characterized by short relaxation times and low viscosities, while systems that respond slowly are characterized by long relaxation times and high viscosities. The relationships are shown by the dual vertical axes in Fig. 1.9, in which larger viscosities correspond to larger values of τ, indicating that decreasing the temperature increases relaxation times. Since glasses are amorphous and supercooled liquids, they are unstable and the relaxation times are of interest in terms of glass formation and kinetics of conversion to crystalline forms.

As seen in Fig. 1.9, the relaxation time or viscosity change drastically at glass transition temperature. As discussed below, the values of T_M, T_g, and the width of T_g range are important parameters in characterizing glasses.

For supercooled liquids, two competing effects are of particular interest. As the temperature is decreased below freezing point, the supercooled liquid becomes thermodynamically less stable with respect to the crystalline form, and the relaxation times become longer as a result of slow diffusion. A major factor that determines

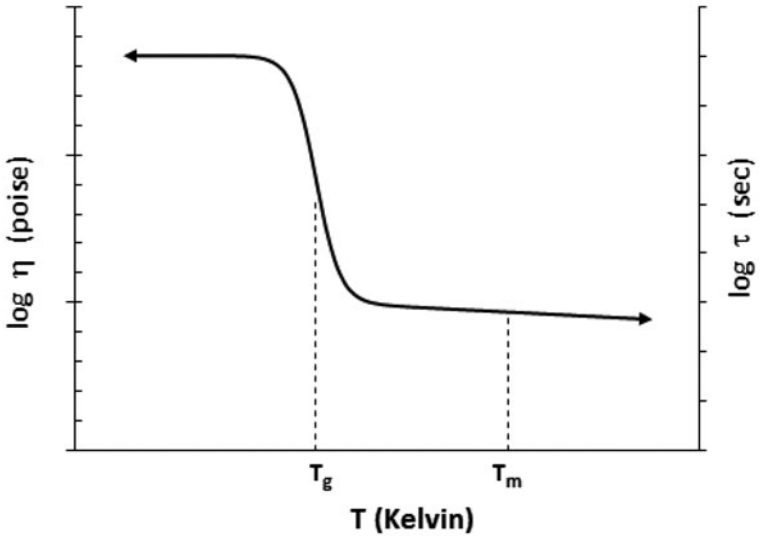

Fig. 1.9 Log η and log τ versus temperature and the glass transition

these effects is the temperature dependency of the relaxation times for the supercooled liquid, and specifically the magnitude of the change in τ with the change in temperature. If the change in relaxation time per change in the temperature is small, the thermodynamic instability of the supercooled melt will result in crystallization over the timeframe of observation. In that case, further cooling is likely to incur crystallization in the observed timeframe, and the supercooled form is less likely to survive. On the other hand, if cooling results in large increases in the relaxation time, crystallization is likely to be slow within the observation timeframe (from minutes to years), and further cooling is unlikely to incur crystallization during that timeframe. These competing effects are further complicated when the cooling rate is considered, since rapid cooling will result in less time for crystallization to occur before the relaxation times are increased. This is discussed further below.

The relationship between the relaxation time and the temperature between glass transition and melting is described by several empirical equations. The one of the most commonly employed Vogel–Fulcher–Tamman (VFT) equation is given by (Mauro et al. 2009; Yu 2001)

$$\tau = \tau_0 \exp\left[\frac{DT_0}{T - T_0}\right] \log \tau = \log \tau_0 + \frac{DT_0}{2.303(T - T_0)}, \tag{1.25}$$

where D is referred to as the strength parameter, T_0 is referred to as the Vogel temperature, and τ_0 is a reference relaxation time corresponding theoretical temperatures approaching infinity. In practice, all three parameters are obtained from fits of the data between T_g and T_M using viscosity or dielectric relaxation time, etc. For many materials, the relaxation times at the glass transition temperature are approximately

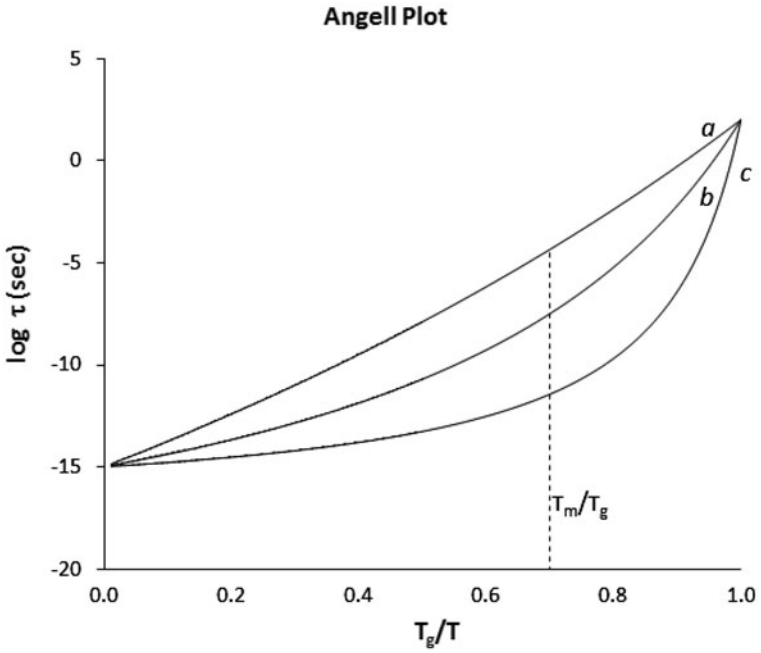

Fig. 1.10 Example of an Angell plot for typical glasses. *Line a* represents a strong glass former ($m = 25$), *b* represents a medium glass former ($m = 50$), and *c* represents a weak glass former ($m = 150$)

$\tau(T_g) \approx 100\ s$, which sets the reference relaxation time $\log \tau_0 \approx 15$. For many materials, D has been related to the Vogel and glass transition temperatures by the empirical equation

$$T_g/T_0 \approx 1 + D/39.1. \tag{1.26}$$

Using this equation, it is possible to correlate the relaxation time and the temperature between T_g and T_M by constructing an Angell plot (Angell 1995; Donth 2001), which plots log τ versus T_g/T. Angell plots give information about the temperature sensitivity of the relaxation time near or above the glass transition temperature. Figure 1.10 shows hypothetical data for three glass formers, each with glass transitions and melting temperatures of 45 and 175 °C. Thus, T_g/T (in Kelvin) ranges from approximately 0.7 to 1.0 in the plot. As the temperature is decreased (moving to the right in the plot), the material represented by line *a* increases its relaxation times much more slowly than the material represented by line *c*. Line *b* represents an intermediate case. Of special interest is the slope of the plot as T_g/T approaches 1, which corresponds to the temperature range in which vitrification occurs. The slope of line at $T_g/T = 1$ is called the fragility *m,* which is formally defined as (Donth 2001):

$$m = \left. \frac{d \log \tau}{d(T_g/T)} \right|_{T=T_g}. \tag{1.27}$$

From Fig. 1.10, line *a* has lowest fragility ($m = 25$) while line *c* has the largest ($m = 150$). Glasses are termed as strong if $m < 40$ or so, and weak if $m > 75$ or so. The significance of the terms is apparent from the Angell plot. As noted above, supercooled melts are thermodynamically unstable, but the crystallization kinetics is affected by the relaxation time. For weak glass formers with large fragility values, the relaxation time remains short until the temperature is lowered close to the T_g so more molecular mobility is retained at lower temperatures, thus making crystallization more likely before the glass transition is reached. In other words, larger values of m are associated with melts that are kinetically more likely to crystallize and less likely to form glasses or amorphous solids.

The fragility can be related to the strength factor and glass transition for typical materials by applying the derivative in Eq. (1.27) to Eq. (1.25), which gives

$$m = \frac{D(T_g/T_0)}{2.303(T_g/T_0 - 1)^2}. \tag{1.28}$$

Applying Eq. (1.26) leads to

$$m \approx 684 \left(\frac{1}{D} + \frac{1}{39.1} \right), \tag{1.29}$$

which can be applied to many typical materials. From Eq. (1.29), it can be said that strong glass formers are associated with strength factors $D > 25$–30 and weak ones with $D < 10$–12.

Numerous publications refer to the association between strong glass formers and Arrhenius-like behavior, as opposed to weak glass formers and non-Arrhenius behaviors (Angell 1995; Yu 2001). While this distinction is not critical for understanding the temperature effects, it is of interest and warrants a short discussion. Arrhenius behavior is associated with systems in which a plot of $\log \tau$ versus $1/T$ (or equivalently, T_g/T) is linear. In the context of Angell plots, the temperature range is from T_g to 50–100°C above T_g. Equation (1.25) shows that this linearity approximately occurs when $1/(T - T_0) \sim 1/T$, or $T/T_0 > 2 - 3$. This is the case for strong glass formers, since for $D > 40$ the value of $T_g/T > 2$, and is higher for any temperature above the glass transition. On the other hand, for weak glass formers with $D < 10$, $T_g/T < 1.25$, and the plots will show curvature (non-Arrhenius behavior).

Consistent with the above discussions, the ability to form glasses depends on the experimental conditions. For instance, while it is possible to supercool a melt for most materials, many materials tend to crystallize near the melting temperature, and will form supercooled melts only if relatively high cooling rates are employed. This is because the conversion of supercooled melt to more stable crystalline forms occurs as a function of relaxation times, in which shorter relaxation times make crystallization

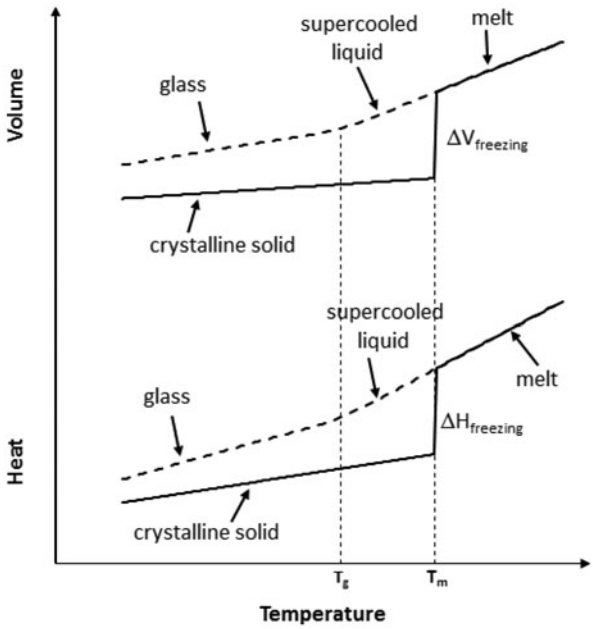

Fig. 1.11 Relationship between the temperature, volume, and heat for glasses and crystalline materials

more likely to occur. If a melt is cooled slowly, the relaxation times also increases slowly and the supercooled melt will have longer timeframes to crystallize. On the other hand, rapid cooling will increase the relaxation times faster than the material can crystallize. If cooled fast enough, the relaxation time of the supercooled melt will become very long before crystallization occurs, so vitrification occurs and a glass will form.

An interesting observation with most glasses is that the behavior on cooling is different from heating. This is a consequence of the fact that nucleation is favored at lower temperatures, while growth is more favored at higher temperatures, but both are very slow at low enough temperatures. Thus, on cooling, it is possible for the temperatures where nucleation is most favored to be below the temperatures where growth is favored, so nucleation without growth may occur. Conversely, on heating the nucleation phase is encountered before the growth phase, so nuclei are present with the growth is most favored. Thus, cooling tends to favor formation of glasses and amorphous forms for systems that behave in this manner.

1.5.1 Thermodynamic Implications of the Glass Transition

Although the glass transition is not a thermodynamic transition in a sense of phase transitions such as crystallization or melting, it provides important thermodynamic

implications. Experimentally, there is an abrupt change in the slope of such properties as molar volume or heat content at the glass transition temperature, while the properties themselves are continuous. Examples of the changes in volume and heat are shown in Fig. 1.11. In the top half, the solid line represents a melting phase transition for a crystalline solid, which shows an abrupt change in the volume at the melting temperature T_M. The dashed plot above it represents the behavior of a melt that forms a supercooled liquid when the temperature is cooled below T_M. It shows a decrease in the magnitude of the slope of V vs. T at the glass transition temperature T_g. Directly below the volume plot is a plot of the heat content vs. T. Again, there is a drop in the heat content at the phase transition temperature, but at the glass transition temperature the slope changes while the heat content is continuous.

This behavior has important energetic consequences. When cooled to below melting temperature, there is an abrupt decrease in the volume and loss of heat if the material undergoes crystallization. If supercooled without crystallization, there is no abrupt decrease in the volume or the heat, which are thus higher than the crystalline solid. The significance of this observation is that the average distance between molecules is larger in a glassy state than in a crystalline state at the same temperature and pressure. A similar analysis can be made for the heat content. Since the supercooled liquid and glassy state do not experience abrupt decreases in the heat content on freezing, the heat content is higher in supercooled form than in the crystalline form at the same (T, P).

These observations can be interpreted in terms the energy versus separation plot of Fig. 1.8. At a given temperature below the melting point, the average separation between molecules and the heat content are both greater in the glassy state than in crystalline forms. As a result, the total energy is higher for the amorphous form than the crystalline form at a given temperature, and the energy needed to reach the dispersive region from the amorphous form is less. As discussed in the next section, this indicates that glassy forms have higher energy and are expected to dissolve more readily than crystalline forms.

1.6 Implications for Solubility and Dissolution

In drug delivery, the primary purpose for considering amorphous drug forms is to increase the solubility and/or dissolution rate of a drug in aqueous media. For amorphous solids, the lack of long-range order has the consequence that the molecular packing is less efficient than crystalline forms, resulting in a larger average molecular separation and weaker attractive forces between molecules. Thus, for a given temperature or heat content, the total energy per amount of material is higher for amorphous than crystalline forms, and the energy required to reach the melt state (level B in Fig. 1.8) and the dispersive region is less for amorphous than crystalline forms.

The lower energy requirements for amorphous solids to reach the dispersive region result in faster dissolution and higher solubility. At a constant temperature, the source

of heat in dissolution is the solvation energy. A simple picture of solvation is that solvent molecules "attach" to undissolved drug molecules, and kinetic energy from the solvent molecules is transferred to a drug–solvent complex. The transfer of energy is a function of the attraction between the drug and solvent, and the number of solvent molecules that transfer energy to the undissolved drug. If the transferred kinetic energy is sufficient to overcome the drug–drug attractions, the drug molecule will leave the undissolved environment and move into the solvent, where it will be surrounded by more solvent molecules and go into solution. Once in solution, the drug molecules can disperse in the solvent, and they are in the dispersive region shown in Fig. 1.8.

With this picture in mind, any modification to the undissolved form that reduces the drug–drug attractive forces reduces the energy needed for "undissolved" molecules to become dissolved forms. At a given temperature, this can be achieved either by increasing the average distance between molecules, which will reduce the magnitude of the attractive forces, or by reducing the number of nearest neighbors. Both will make the total energy experienced by a molecule less negative and reduce the energy needed from the solvent to reach the dispersion region.

The first can be achieved by creating amorphous forms. By increasing the average distance between molecules, the attractive energy is less negative and the total energy increases. In addition, different polymorphic forms represent different molecular packing arrangements, and can reduce the number of nearest neighbor molecules. Since the total attractive energy is additive, creating arrangements with fewer nearest neighbors reduces the number of interactions and makes the total energy less negative.

Another way to reduce the number of nearest neighbors is by increasing the total surface area per volume, since molecules on surface lack the molecules above the surface. In addition, for extremely small particles (for instance, nuclei with radii of curvature less than 10 nm), the number of molecules per volume is reduced due to steric hindrance. This is one source of the Kelvin effect, in which the solubility of a substance increases with decreasing radius of curvature (Adamson and Gast 1997).

A third method to reduce the energy needed to reach the dispersive region is by inserting excipient molecules between the drug molecules, in which the drug–excipient interactions are weaker than the drug–drug interactions, or excipient–water interactions are stronger than drug–water interactions. The first case reduces the energy required to displace the drug and reach the dispersive region, and the second increases the energy obtained from the water–excipient interactions to dissolve the drug molecules. This is the basis for ASDs, which will be covered in subsequent chapters.

For a given drug and solvent, a kinetic view of dissolution can be formed. The "undissolved" solid with weak drug–drug attractions will allow the drug to leave from the solid more readily than one with stronger interaction. Kinetically, this corresponds to a lower energy barrier, which can approximately be thought of as the energy required to remove a drug molecule from its "undissolved" solid. Since dissolution occurs when drugs leave a solid surface, the specific energy that must be considered is the surface energy, which is related to the bulk energy by relationships such as the Scapski–Turnbull rule (Adamson and Gast 1997). Since the rate at which

molecules leave the surface often follows an Arrhenius relationship, the dissolution rate can be related to the energy barrier ε_a as

$$\text{Dissolution rate} \propto \exp\left(-\frac{\varepsilon_a}{k_B T}\right). \tag{1.30}$$

Of course, the dissolution rate also depends on other factors such as the diffusion coefficient of the drug in the solvent, stirring, etc. However, if the energy barrier is large, then the rate-limiting step for dissolution is the removal of the drug from the surface of the undissolved solid. In that case, Eq. (1.30) can describe surface limited dissolution, as opposed to diffusion-limited dissolution. (This is a topic of some debate, as some pharmaceutical scientists claim that surface limited dissolution does not occur in practice.)

1.7 Implications for Physical Stability

Amorphous forms show a tendency toward crystallization as the means to reduce the total energy content. The rate of conversion must be slow enough to provide an intended shelf life for amorphous forms to be commercially viable. In a pure substance, crystallization may occur after short translational motions; whereas in ASD, longer diffusion motions are required. In this sense, pure amorphous forms convert to crystalline forms more rapidly than ASD's. The following illustrates the order of magnitude of the molecular motions on crystallization.

For a neat substance with a true density of ρ_0 (g/cm) and molecular weight M (g/mole), the average distance between drug molecules $\langle r \rangle$ can be estimated as

$$\langle r \rangle = \left(\frac{M}{\rho_0 N_A}\right)^{1/3}, \tag{1.31}$$

where N_A represents Avogadro's number (6.02×10^{23} molecules per mole). Also, Eq. (1.31) shows $\langle r \rangle \propto (1/\rho_0)^{1/3}$. As examples, the average distance between water molecules in the liquid state is $\langle r \rangle \sim 0.31nm$, while for ice ($\rho_0 = 0.917 g/cm^3$) it is $\langle r \rangle \sim 0.32nm$, or about 3 % larger than for liquid water. For solid ibuprofen, ρ_0 is close to 1 g/cm^3 (D'Arcy and Persoons 2011) and the calculated average separation is $\langle r \rangle \sim 0.7nm$. Since the relative density differences between polymorphs and amorphous forms are small, the relative changes in average molecular separations are small as well. Thus, crystallization of amorphous forms involves short range motions or rearrangements of molecules that are typically shorter than 0.1 nm.

The main energy barrier to crystallization for pure amorphous materials is rotational, not diffusional. The kinetics of crystallization depend on the ability of the molecules to come into proximity plus to overcome energy barriers associated with going through intermediate arrangements to achieve the optimal structural alignment (the crystalline arrangement). For neat amorphous forms, the molecules are already in close proximity, so the second step is more important. In comparison, the average

distance between drug molecules is larger in ASD's. Thus, the motions required for crystallization to occur in ASD's are significantly larger. In addition, in a solid solution ASD, the drug molecules are separated both by a large distance and have excipient molecules (polymers) between them. Thus, crystallization must occur after diffusion, which slows the overall process of losing the amorphous nature.

1.8 Kinetic Considerations

As discussed earlier in Sect. 1.5, the relaxation time of amorphous material is increased as the temperature is decreased. The Angell plot (Fig. 1.10) gives details of the temperature sensitivity for supercooled liquids between the melt and the glass transition temperatures, but in general it does not extend to lower temperatures for which $T_g/T > 1$. In fact, the extrapolations below the glass transition temperature often fail and the methods to determine the exact forms of equations for extrapolation are still being studied actively (Garca-Coln et al. 1989; Trachenko 2008; Mauro et al. 2009). Still, as would be expected, the relaxation time will continue to increase in some manner. As noted earlier, the relaxation time at the glass transition temperature for many materials is approximately $\tau(T_g) \approx 100s(\log \tau = 2)$, which is long enough for most organic molecules to undergo some crystallization within reasonably short timeframes.

It will be useful to estimate how far from the glass transition temperature an amorphous material can be stored to ensure that the material is kinetically stable over the duration of shelf life. Several rules of thumb have been proposed, of which probably the best known is the "$T_g - 50$ rule" for estimating the required storage temperature (Hancock et al. 1995). If this temperature is far below room temperature, storage of the amorphous drug at that temperature will not be practical, and alternative means of stabilizing the amorphous drug will be needed. (It should be noted that the "$T_g - 50$ rule" is a generalization based on concepts such as those detailed above. While many materials do not follow this rule, it is still a useful concept.)

The kinetics of crystallization has been simulated by many models, including the Avrami model (House 2007). The rate of conversion from amorphous to crystalline states can be measured by using thermal analysis (differential scanning calorimetry, DSC) and/or X-ray diffraction. The rate of conversion from amorphous to crystalline form depends on a number of factors. The process occurs in two steps, nucleation and growth (Mullin 2001), which are affected by various factors and occur at different rates. Specifically, for crystallization to occur, a seed or nucleus must form, on which subsequent growth will occur. Thus, the rate of nucleation is of primary interest. By analogy with Arrhenius-type processes, the nucleation rate can be written as

$$\frac{dN_{\text{nuc}}}{dt} = A \exp\left[-\frac{\Delta g_{\text{cr}}}{k_B T}\right], \tag{1.32}$$

where $\mathrm{d}N_{\text{nuc}}/\mathrm{d}t$ denotes the number of nuclei formed per volume per time, and Δg_{cr} reflects an activation energy for nucleation. This activation energy is related to

the interfacial energy between a crystallizing nucleus and surrounding amorphous medium, and thus depends on the particle size via its surface area. For the idealized case of a spherical nucleus, the change in Gibbs energy with formation of a particle depends on the environment. For instance, when nucleation occurs from a supersaturated solution of a drug in a liquid solvent, Δg_{cr} and the nucleation rate are given by

$$\Delta g_{cr} = \frac{16\pi v^2 \gamma^3}{3(k_B T \ln S)^2} \text{ and } \frac{dN_{nuc}}{dt} = A \exp\left[-\frac{16\pi v^2 \gamma^3}{3k_B^3 T^3 (\ln S)^2}\right], \tag{1.33}$$

where v is the molecular volume, γ is the interfacial tension of the nuclei in the amorphous environment, and S is the degree of supersaturation. On the other hand, if nucleation occurs from the melt of a pure substance, these are given by (Mullin 2001; Adamson and Gast 1997):

$$\Delta g_{cr} = \frac{16\pi v^2 \gamma^3 T_M^2}{3\Delta h_M^2 (T_M - T)^2} \text{ and } \frac{dN_{nuc}}{dt} = A \exp\left[-\frac{16\pi v^2 \gamma^3 T_M^2}{3k_B T \Delta h_M^2 (T_M - T)^2}\right], \tag{1.34}$$

where, γ represents the interfacial tension between the crystalline form and the melt. In an amorphous solid, it can be expected that nucleation will follow a pattern analogous to Eq. (1.34), in which γ would represent the interfacial tension between the crystalline and amorphous forms of the drug. This reflects the notion that a pure API is not microscopically homogeneous when nucleation and crystallization are occurring, so on a microscopic scale, there are regions with different molecular packing, density, and energy patterns. These regions create interfaces and interfacial tensions, based on the different molecular packing of the regions.

Because of the interfacial terms in Eq. (1.34), nucleation is sometimes modeled as occurring randomly in pure amorphous materials. This is one of the central assumptions of models for crystallization kinetics, and has led to solid-state kinetic models such as the Prout–Tompkins and Avrami models (House 2007), in which crystallization is modeled as random nucleation events in location and time, followed by growth by a definable mechanism. For instance, in 2-d and 3-d growth models, nucleation is treated as occurring at a constant rate per unconverted (amorphous) fraction of the sample volume, followed by a growth rate that is approximated as being constant along a given dimension such as the radius. This leads to an expression of a general Avrami equation (also known as the Avrami-Erofe'ev, or Johnson-Mehl-Avrami equations), given by

$$\alpha = 1 - \exp(-kt^n), \tag{1.35}$$

where α represents the fraction of a sample that has been converted to crystalline form, k is a function of several physical variables, and n is a function of the geometry (plates, spheres, etc.) for the growing crystals. The parameters k and n can be obtained from nonlinear fits of the data, or classic double log plots such as

$$\ln[-\ln(1 - \alpha)] = \ln k + n \ln t. \tag{1.36}$$

An example calculation will illustrate the approach. If the number of nuclei formed per time per unconverted volume is denoted by a constant rate $\dot{N}_0$, the number of nuclei that form in a sample between times τ and $\tau + d\tau$ is $\dot{N}_0 V_T(1-\alpha)d\tau$. Here, V_T denotes the total sample volume, V is the volume that has converted to the crystalline form, and $\alpha = V/V_T$. The crystals are assumed to form perfect spheres of volume $4\pi r^3/3$, and the interfacial energy between the crystals and surrounding amorphous material is assumed to be constant (which is reasonable once crystals grow to larger than several nanometers in radius), so the radius of each sphere can be assumed to increase at the same constant rate $\dot{r}_0$. With these assumptions, the size of a sphere at a time t that formed at time between τ and $\tau + d\tau$ would be $4\pi\dot{r}_0^3(t-\tau)^3/3$. Also, at time t the total volume occupied by all spheres formed volume occupied by all spheres formed between τ and $\tau + d\tau$, denoted by $dV(t,\tau)$, would be the volume of each times the number that formed in that time interval, or

$$dV(t,\tau) = \frac{4\pi\dot{r}_0^3}{3}(t-\tau)^3 \times V_T(1-\alpha) \times \dot{N}_0 d\tau, \tag{1.37}$$

which can be rewritten as

$$\frac{d\alpha}{(1-\alpha)} = \frac{4\pi\dot{r}_0^3\dot{N}_0}{3}(t-\tau)^3 d\tau. \tag{1.38}$$

At any time, $\alpha(t)$ can be found by integrating both sides. Assuming no converted fraction initially, the left-hand side is integrated from 0 to α and the right-hand side is integrated over all formation times τ from 0 to the observation time *t,* which leads to

$$\ln(1-\alpha) = \frac{\pi\dot{r}_0^3\dot{N}_0 t^4}{3} \tag{1.39}$$

or

$$\alpha = 1 - exp(-kt^4) \quad k = \frac{\pi\dot{r}_0^3\dot{N}_0}{3}. \tag{1.40}$$

This form of the Avrami equation describes a uniform 3-d growth of spherical particles whose nuclei randomly form at a constant average rate per unconverted volume, and is of a mathematical form referred to as the Avrami (A4) nucleation model (Khawam and Flanagan 2006). Other forms for other growth patterns have been derived, such as for crystals that grow as disks as (House 2007)

$$\alpha = 1 - exp(-kt^3) \quad k = \frac{\pi\dot{r}_0^3\dot{N}_0}{3}. \tag{1.41}$$

These equations have been successfully used in practice to model crystallization data. Since equations have been derived for a number of Avrami models, this approach has the advantage that the model does not have to be known a priori, but instead can be chosen based on which equations fit the data (along with some physical insight). It is also possible to perform experiments at different temperatures or under nonisothermal conditions to facilitate further analyses such as obtaining growth activation energies, and the reader is referred to other works for detailed treatments (Khawam and Flanagan 2006).

1.9 Summary and Closing Remarks

Amorphous solids have been of great interest to pharmaceutical scientists for decades. Their potential for increasing bioavailability is of great importance, although they have not been utilized to the full potential to date. In this chapter, the thermodynamic and molecular foundation of neat amorphous APIs were presented with the goal of relating these properties to possible dissolution and solubility advantages, as well as to shed light on physical instability. Some kinetic considerations on amorphous materials were also presented because of their practical importance.

It is the opinion of this author that neat amorphous API and ASD formulations show great promise for future applications, but their utilization has not fully materialized due to a lack of understanding of how the systems work. The fact that the approach of using amorphous forms for drug delivery has been studied for nearly five decades and still yet not used in more drug products is indicative of the nature of the problem. Studying amorphous forms for drug delivery is interdisciplinary in nature, and requires high levels of expertise in fields ranging from pharmacy to chemistry, biology, physics and computer science. We are in exciting times because experimental equipment and computational platforms are rapidly increasing our fundamental knowledge of material science. Looking forward, it seems inevitable that these forms will find more commercial applications in drug delivery in the not-too-distant future.

Acknowledgments I would like to thank Drs. Navnit Shah, Harpreet Sandhu, and Duk Soon Choi for their invaluable interactions over the past several years. I would also like to especially thank Drs. Kosha Shah and Piyush Patel, with whom I have had countless scientific conversations and who have kept me on track when I was overwhelmed with commitments.

References

Adamson AW, Gast AP (1997) Physical chemistry of surfaces, 6th edn. Wiley, New York

Adjei A, Newburger J, Martin A (1980) Extended Hildebrand approach: solubility of caffeine in dioxane-water mixtures. J Pharm Sci 69:659–661

Amidon GL, Lennernäs H, Shah VP, Crison JR (1995) A theoretical basis for a biopharmaceutic drug classification: the correlation of in vitro drug product dissolution and in vivo bioavailability. Pharm Res 12:413–420

Angell CA (1995) Formation of glasses from liquids and biopolymers. Science 267:1924–1935

Atkins PW (1998) Physical chemistry, 6th edn. Freeman, New York

Bellantone RA, Patel P, Sandhu H, Choi D, Singhal D, Chokshi H, Malick AW, Shah NH (2012) A method to predict the equilibrium solubility of drugs in solid polymers near room temperature using thermal analysis. J Pharm Sci 101:4549–4558

Burger A, Ramberger R (1979) On the polymorphism of pharmaceutical and other molecular crystals I. Theory of thermodynamic rules. Mikrochimica Acta 11:259–281

Chiou WL, Riegelman S (1971) Pharmaceutical applications of solid dispersion systems. J Pharm Sci 60:1281–1302

D'Arcy DM, Persoons T (2011) Mechanistic modelling and mechanistic monitoring: simulation and shadowgraph imaging of particulate dissolution in the flow-through apparatus. J Pharm Sci 100:1102–1115

Donth E (2001) The glass transition: relaxation dynamics in liquids and disordered materials. Springer, Berlin
Garca-Coln LS, del Castillo LF, Goldstein P (1989) Theoretical basis for the Vogel-Fulcher-Tammann equation. Phys Rev B 40:7040–7044
Gavezzotti A (2007) Molecular aggregation: structure analysis and molecular simulation of crystals and liquids. Oxford University Press, New York (Chap. 14)
Hancock BC, Zografi G (1997) Characteristics and significance of the amorphous state in pharmaceutical systems. J Pharm Sci 86:1–12
Hancock BC, Shamblin SL, Zografi G (1995) Molecular mobility of amorphous pharmaceutical solids below their glass transition temperatures. Pharm Res 12:799–806
Herschler B, Humer C (2012) FDA new drug approvals hit 16-year high in 2012. Reuters Online. 2012. http://www.reuters.com/article/2012/12/31/us-pharmaceuticals-fda-approvals-idUSBRE8BU0EK20121231. Accessed 31 Dec 2012
Hildebrand J, Scott R (1950) Solubility of non-electrolytes, 3rd edn. Rheinhold, New York
Hill TL (1986) An introduction to statistical thermodynamics. Dover, New York
House JE (2007) Principles of chemical kinetics, 2nd edn. Elsevier, Amsterdam
Khawam A, Flanagan DR (2006) Basics and applications of solid state kinetics: a pharmaceutical perspective. J Pharm Sci 95:472–498
Kittel C (1986) Introduction to solid state physics, 6th edn. Wiley, New York
Klotz IM, Rosenberg RM (1974) Chemical thermodynamics—basic theory and methods, 3rd edn. Benjamin-Cummings, New York
Klug HP, Alexander LE (1974) X-ray diffraction procedures for polycrystalline and amorphous materials. Wiley, New York
Leuner C, Dressman J (2002) Improving drug solubility for oral delivery using solid dispersions. Eur J Pharm Biopharm 50:47–60
Martin A, Swarbrick J, Cammarata A (1983) Physical pharmacy, 3rd edn. Lea & Febiger, Philadelphia
Mauro JC, Yue Y, Ellison AJ, Gupta PK, Allan DC (2009) Viscosity of glass-forming liquids. Proc Natl Acad Sci 106:19780–19784
Mullin JW (2001) Crystallization, 4th edn. Butterworth-Heinemann, Boston
Simonelli AP, Mehta SC, Higuchi WI (1969) Dissolution rates of high energy polyvinyl pyrrolidone (PVP)-sulfathiazole coprecipitates. J Pharm Sci 58:538–549
Trachenko K (2008) The Vogel–Fulcher–Tammann law in the elastic theory of glass transition. J Non-cryst Solids 354:3903–3906
Williams RO III, Watts AB, Miller DA (eds) (2012) Formulating poorly water soluble drugs. Springer, New York (Preface)
Yu L (2001) Amorphous pharmaceutical solids: preparation, characterization and stabilization. Adv Drug Del Rev 48:27–42